

Study of the Dalitz decay $J/\psi \rightarrow e^+ e^- \eta$

M. Ablikim,¹ M. N. Achasov,^{9,d} S. Ahmed,¹⁴ M. Albrecht,⁴ M. Alekseyev,^{55a,55c} A. Amoroso,^{55a,55c} F. F. An,¹ Q. An,^{52,42} Y. Bai,⁴¹ O. Bakina,²⁶ R. Baldini Ferroli,^{22a} Y. Ban,³⁴ K. Begzsuren,²⁴ D. W. Bennett,²¹ J. V. Bennett,⁵ N. Berger,²⁵ M. Bertani,^{22a} D. Bettoni,^{23a} F. Bianchi,^{55a,55c} E. Boger,^{26,b} I. Boyko,²⁶ R. A. Briere,⁵ H. Cai,⁵⁷ X. Cai,^{1,42} O. Cakir,^{45a} A. Calcaterra,^{22a} G. F. Cao,^{1,46} S. A. Cetin,^{45b} J. Chai,^{55c} J. F. Chang,^{1,42} W. L. Chang,^{1,46} G. Chelkov,^{26,b,c} G. Chen,¹ H. S. Chen,^{1,46} J. C. Chen,¹ M. L. Chen,^{1,42} P. L. Chen,⁵³ S. J. Chen,³² X. R. Chen,²⁹ Y. B. Chen,^{1,42} X. K. Chu,³⁴ G. Cibinetto,^{23a} F. Cossio,^{55c} H. L. Dai,^{1,42} J. P. Dai,^{37,h} A. Dbeyssi,¹⁴ D. Dedovich,²⁶ Z. Y. Deng,¹ A. Denig,²⁵ I. Denysenko,²⁶ M. Destefanis,^{55a,55c} F. De Mori,^{55a,55c} Y. Ding,³⁰ C. Dong,³³ J. Dong,^{1,42} L. Y. Dong,^{1,46} M. Y. Dong,^{1,42,46} Z. L. Dou,³² S. X. Du,⁶⁰ P. F. Duan,¹ J. Fang,^{1,42} S. S. Fang,^{1,46} Y. Fang,¹ R. Farinelli,^{23a,23b} L. Fava,^{55b,55c} S. Fegan,²⁵ F. Feldbauer,⁴ G. Felici,^{22a} C. Q. Feng,^{52,42} E. Fioravanti,^{23a} M. Fritsch,⁴ C. D. Fu,¹ Q. Gao,¹ X. L. Gao,^{52,42} Y. Gao,⁴⁴ Y. G. Gao,⁶ Z. Gao,^{52,42} B. Garillon,²⁵ I. Garzia,^{23a} A. Gilman,⁴⁹ K. Goetzen,¹⁰ L. Gong,³³ W. X. Gong,^{1,42} W. Gradl,²⁵ M. Greco,^{55a,55c} L. M. Gu,³² M. H. Gu,^{1,42} Y. T. Gu,¹² A. Q. Guo,¹ L. B. Guo,³¹ R. P. Guo,^{1,46} Y. P. Guo,²⁵ A. Guskov,²⁶ Z. Haddadi,²⁸ S. Han,⁵⁷ X. Q. Hao,¹⁵ F. A. Harris,⁴⁷ K. L. He,^{1,46} F. H. Heinsius,⁴ T. Held,⁴ Y. K. Heng,^{1,42,46} T. Holtmann,⁴ Z. L. Hou,¹ H. M. Hu,^{1,46} J. F. Hu,^{37,h} T. Hu,^{1,42,46} Y. Hu,¹ G. S. Huang,^{52,42} J. S. Huang,¹⁵ X. T. Huang,³⁶ X. Z. Huang,³² Z. L. Huang,³⁰ T. Hussain,⁵⁴ W. Ikegami Andersson,⁵⁶ M. Irshad,^{52,42} Q. Ji,¹ Q. P. Ji,¹⁵ X. B. Ji,^{1,46} X. L. Ji,^{1,42} X. S. Jiang,^{1,42,46} X. Y. Jiang,³³ J. B. Jiao,³⁶ Z. Jiao,¹⁷ D. P. Jin,^{1,42,46} S. Jin,^{1,46} Y. Jin,⁴⁸ T. Johansson,⁵⁶ A. Julin,⁴⁹ N. Kalantar-Nayestanaki,²⁸ X. S. Kang,³³ M. Kavatsyuk,²⁸ B. C. Ke,¹ T. Khan,^{52,42} A. Khoukaz,⁵⁰ P. Kiese,²⁵ R. Kliemt,¹⁰ L. Koch,²⁷ O. B. Kolcu,^{45b,f} B. Kopf,⁴ M. Kornicer,⁴⁷ M. Kuemmel,⁴ M. Kuessner,⁴ A. Kupsc,⁵⁶ M. Kurth,¹ W. Kühn,²⁷ J. S. Lange,²⁷ M. Lara,²¹ P. Larin,¹⁴ L. Lavezzi,^{55c} S. Leiber,⁴ H. Leithoff,²⁵ C. Li,⁵⁶ Cheng Li,^{52,42} D. M. Li,⁶⁰ F. Li,^{1,42} F. Y. Li,³⁴ G. Li,¹ H. B. Li,^{1,46} H. J. Li,^{1,46} J. C. Li,¹ J. W. Li,⁴⁰ K. J. Li,⁴³ Kang Li,¹³ Ke Li,¹ Lei Li,³ P. L. Li,^{52,42} P. R. Li,^{46,7} Q. Y. Li,³⁶ T. Li,³⁶ W. D. Li,^{1,46} W. G. Li,¹ X. L. Li,³⁶ X. N. Li,^{1,42} X. Q. Li,³³ Z. B. Li,⁴³ H. Liang,^{52,42} Y. F. Liang,³⁹ Y. T. Liang,²⁷ G. R. Liao,¹¹ L. Z. Liao,^{1,46} J. Libby,²⁰ C. X. Lin,⁴³ D. X. Lin,¹⁴ B. Liu,^{37,h} B. J. Liu,¹ C. X. Liu,¹ D. Liu,^{52,42} D. Y. Liu,^{37,h} F. H. Liu,³⁸ Fang Liu,¹ Feng Liu,⁶ H. B. Liu,¹² H. L. Liu,⁴¹ H. M. Liu,^{1,46} Huanhuan Liu,¹ Huihui Liu,¹⁶ J. B. Liu,^{52,42} J. Y. Liu,^{1,46} K. Liu,⁴⁴ K. Y. Liu,³⁰ Ke Liu,⁶ L. D. Liu,³⁴ Q. Liu,⁴⁶ S. B. Liu,^{52,42} X. Liu,²⁹ Y. B. Liu,³³ Z. A. Liu,^{1,42,46} Zhiqing Liu,²⁵ Y. F. Long,³⁴ X. C. Lou,^{1,42,46} H. J. Lu,¹⁷ J. G. Lu,^{1,42} Y. Lu,¹ Y. P. Lu,^{1,42} C. L. Luo,³¹ M. X. Luo,⁵⁹ X. L. Luo,^{1,42} S. Lusso,^{55c} X. R. Lyu,⁴⁶ F. C. Ma,³⁰ H. L. Ma,¹ L. L. Ma,³⁶ M. M. Ma,^{1,46} Q. M. Ma,¹ X. N. Ma,³³ X. Y. Ma,^{1,42} Y. M. Ma,³⁶ F. E. Maas,¹⁴ M. Maggiora,^{55a,55c} Q. A. Malik,⁵⁴ A. Mangoni,^{22b} Y. J. Mao,³⁴ Z. P. Mao,¹ S. Marcelllo,^{55a,55c} Z. X. Meng,⁴⁸ J. G. Messchendorp,²⁸ G. Mezzadri,^{23a} J. Min,^{1,42} T. J. Min,¹ R. E. Mitchell,²¹ X. H. Mo,^{1,42,46} Y. J. Mo,⁶ C. Morales Morales,¹⁴ G. Morello,^{22a} N. Yu. Muchnoi,^{9,d} H. Muramatsu,⁴⁹ A. Mustafa,⁴ S. Nakhoul,^{10,g} Y. Nefedov,²⁶ F. Nerling,^{10,g} I. B. Nikolaev,^{9,d} Z. Ning,^{1,42} S. Nisar,⁸ S. L. Niu,^{1,42} X. Y. Niu,^{1,46} S. L. Olsen,^{35,j} Q. Ouyang,^{1,42,46} S. Pacetti,^{22b} Y. Pan,^{52,42} M. Papenbrock,⁵⁶ P. Patteri,^{22a} M. Pelizaeus,⁴ J. Pellegrino,^{55a,55c} H. P. Peng,^{52,42} Z. Y. Peng,¹² K. Peters,^{10,g} J. Pettersson,⁵⁶ J. L. Ping,³¹ R. G. Ping,^{1,46} A. Pitka,⁴ R. Poling,⁴⁹ V. Prasad,^{52,42} H. R. Qi,² M. Qi,³² T. Y. Qi,² S. Qian,^{1,42} C. F. Qiao,⁴⁶ N. Qin,⁵⁷ X. S. Qin,⁴ Z. H. Qin,^{1,42} J. F. Qiu,¹ K. H. Rashid,^{54,i} C. F. Redmer,²⁵ M. Richter,⁴ M. Ripka,²⁵ M. Rolo,^{55c} G. Rong,^{1,46} Ch. Rosner,¹⁴ X. D. Ruan,¹² A. Sarantsev,^{26,e} M. Savrié,^{23b} C. Schnier,⁴ K. Schoenning,⁵⁶ W. Shan,¹⁸ X. Y. Shan,^{52,42} M. Shao,^{52,42} C. P. Shen,² P. X. Shen,³³ X. Y. Shen,^{1,46} H. Y. Sheng,¹ X. Shi,^{1,42} J. J. Song,³⁶ W. M. Song,³⁶ X. Y. Song,¹ S. Sosio,^{55a,55c} C. Sowa,⁴ S. Spataro,^{55a,55c} G. X. Sun,¹ J. F. Sun,¹⁵ L. Sun,⁵⁷ S. S. Sun,^{1,46} X. H. Sun,¹ Y. J. Sun,^{52,42} Y. K. Sun,^{52,42} Y. Z. Sun,¹ Z. J. Sun,^{1,42} Z. T. Sun,²¹ Y. T. Tan,^{52,42} C. J. Tang,³⁹ G. Y. Tang,¹ X. Tang,¹ I. Tapan,^{45c} M. Tiemens,²⁸ B. Tsednee,²⁴ I. Uman,^{45d} G. S. Varner,⁴⁷ B. Wang,¹ B. L. Wang,⁴⁶ C. W. Wang,³² D. Wang,³⁴ D. Y. Wang,³⁴ Dan Wang,⁴⁶ K. Wang,^{1,42} L. L. Wang,¹ L. S. Wang,¹ M. Wang,³⁶ Meng Wang,^{1,46} P. Wang,¹ P. L. Wang,¹ W. P. Wang,^{52,42} X. F. Wang,¹ Y. Wang,^{52,42} Y. F. Wang,^{1,42,46} Y. Q. Wang,²⁵ Z. Wang,^{1,42} Z. G. Wang,^{1,42} Z. Y. Wang,¹ Zongyuan Wang,^{1,46} T. Weber,⁴ D. H. Wei,¹¹ P. Weidenkaff,²⁵ S. P. Wen,¹ U. Wiedner,⁴ M. Wolke,⁵⁶ L. H. Wu,¹ L. J. Wu,^{1,46} Z. Wu,^{1,42} L. Xia,^{52,42} X. Xia,³⁶ Y. Xia,¹⁹ D. Xiao,¹ Y. J. Xiao,^{1,46} Z. J. Xiao,³¹ Y. G. Xie,^{1,42} Y. H. Xie,⁶ X. A. Xiong,^{1,46} Q. L. Xiu,^{1,42} G. F. Xu,¹ J. J. Xu,^{1,46} L. Xu,¹ Q. J. Xu,¹³ Q. N. Xu,⁴⁶ X. P. Xu,⁴⁰ F. Yan,⁵³ L. Yan,^{55a,55c} W. B. Yan,^{52,42} W. C. Yan,² Y. H. Yan,¹⁹ H. J. Yang,^{37,h} H. X. Yang,¹ L. Yang,⁵⁷ S. L. Yang,^{1,46} Y. H. Yang,³² Y. X. Yang,¹¹ Yifan Yang,^{1,46} M. Ye,^{1,42} M. H. Ye,⁷ J. H. Yin,¹ Z. Y. You,⁴³ B. X. Yu,^{1,42,46} C. X. Yu,³³ J. S. Yu,²⁹ C. Z. Yuan,^{1,46} Y. Yuan,¹ A. Yuncu,^{45b,a} A. A. Zafar,⁵⁴ A. Zallo,^{22a} Y. Zeng,¹⁹ Z. Zeng,^{52,42} B. X. Zhang,¹ B. Y. Zhang,^{1,42} C. C. Zhang,¹ D. H. Zhang,¹ H. H. Zhang,⁴³ H. Y. Zhang,^{1,42} J. Zhang,^{1,46} J. L. Zhang,⁵⁸ J. Q. Zhang,⁴ J. W. Zhang,^{1,42,46} J. Y. Zhang,¹ J. Z. Zhang,^{1,46} K. Zhang,^{1,46} L. Zhang,⁴⁴ S. F. Zhang,³² T. J. Zhang,^{37,h} X. Y. Zhang,³⁶ Y. Zhang,^{52,42} Y. H. Zhang,^{1,42} Y. T. Zhang,^{52,42} Yang Zhang,¹ Yao Zhang,¹ Yu Zhang,⁴⁶ Z. H. Zhang,⁶ Z. P. Zhang,⁵² Z. Y. Zhang,⁵⁷ G. Zhao,¹ J. W. Zhao,^{1,42} J. Y. Zhao,^{1,46} J. Z. Zhao,^{1,42} Lei Zhao,^{52,42} Ling Zhao,¹ M. G. Zhao,³³ Q. Zhao,¹ S. J. Zhao,⁶⁰ T. C. Zhao,¹ Y. B. Zhao,^{1,42} Z. G. Zhao,^{52,42} A. Zhemchugov,^{26,b} B. Zheng,⁵³ J. P. Zheng,^{1,42} W. J. Zheng,³⁶ Y. H. Zheng,⁴⁶ B. Zhong,³¹ L. Zhou,^{1,42} Q. Zhou,^{1,46} X. Zhou,⁵⁷ X. K. Zhou,^{52,42}

X. R. Zhou,^{52,42} X. Y. Zhou,¹ A. N. Zhu,^{1,46} J. Zhu,³³ J. Zhu,⁴³ K. Zhu,¹ K. J. Zhu,^{1,42,46} S. Zhu,¹ S. H. Zhu,⁵¹ X. L. Zhu,⁴⁴
 Y. C. Zhu,^{52,42} Y. S. Zhu,^{1,46} Z. A. Zhu,^{1,46} J. Zhuang,^{1,42} B. S. Zou,¹ and J. H. Zou¹

(BESIII Collaboration)

- ¹*Institute of High Energy Physics, Beijing 100049, People's Republic of China*
²*Beihang University, Beijing 100191, People's Republic of China*
³*Beijing Institute of Petrochemical Technology, Beijing 102617, People's Republic of China*
⁴*Bochum Ruhr-University, D-44780 Bochum, Germany*
⁵*Carnegie Mellon University, Pittsburgh, Pennsylvania 15213, USA*
⁶*Central China Normal University, Wuhan 430079, People's Republic of China*
⁷*China Center of Advanced Science and Technology, Beijing 100190, People's Republic of China*
⁸*COMSATS Institute of Information Technology, Lahore, Defence Road, Off Raiwind Road, 54000 Lahore, Pakistan*
⁹*G.I. Budker Institute of Nuclear Physics SB RAS (BINP), Novosibirsk 630090, Russia*
¹⁰*GSI Helmholtzcentre for Heavy Ion Research GmbH, D-64291 Darmstadt, Germany*
¹¹*Guangxi Normal University, Guilin 541004, People's Republic of China*
¹²*Guangxi University, Nanning 530004, People's Republic of China*
¹³*Hangzhou Normal University, Hangzhou 310036, People's Republic of China*
¹⁴*Helmholtz Institute Mainz, Johann-Joachim-Becher-Weg 45, D-55099 Mainz, Germany*
¹⁵*Henan Normal University, Xinxiang 453007, People's Republic of China*
¹⁶*Henan University of Science and Technology, Luoyang 471003, People's Republic of China*
¹⁷*Huangshan College, Huangshan 245000, People's Republic of China*
¹⁸*Hunan Normal University, Changsha 410081, People's Republic of China*
¹⁹*Hunan University, Changsha 410082, People's Republic of China*
²⁰*Indian Institute of Technology Madras, Chennai 600036, India*
²¹*Indiana University, Bloomington, Indiana 47405, USA*
^{22a}*INFN Laboratori Nazionali di Frascati, I-00044, Frascati, Italy*
^{22b}*INFN and University of Perugia, I-06100, Perugia, Italy*
^{23a}*INFN Sezione di Ferrara, I-44122, Ferrara, Italy*
^{23b}*University of Ferrara, I-44122, Ferrara, Italy*
²⁴*Institute of Physics and Technology, Peace Ave. 54B, Ulaanbaatar 13330, Mongolia*
²⁵*Johannes Gutenberg University of Mainz, Johann-Joachim-Becher-Weg 45, D-55099 Mainz, Germany*
²⁶*Joint Institute for Nuclear Research, 141980 Dubna, Moscow region, Russia*
²⁷*Justus-Liebig-Universitaet Giessen, II. Physikalisches Institut, Heinrich-Buff-Ring 16, D-35392 Giessen, Germany*
²⁸*KVI-CART, University of Groningen, NL-9747 AA Groningen, The Netherlands*
²⁹*Lanzhou University, Lanzhou 730000, People's Republic of China*
³⁰*Liaoning University, Shenyang 110036, People's Republic of China*
³¹*Nanjing Normal University, Nanjing 210023, People's Republic of China*
³²*Nanjing University, Nanjing 210093, People's Republic of China*
³³*Nankai University, Tianjin 300071, People's Republic of China*
³⁴*Peking University, Beijing 100871, People's Republic of China*
³⁵*Seoul National University, Seoul, 151-747 Korea*
³⁶*Shandong University, Jinan 250100, People's Republic of China*
³⁷*Shanghai Jiao Tong University, Shanghai 200240, People's Republic of China*
³⁸*Shanxi University, Taiyuan 030006, People's Republic of China*
³⁹*Sichuan University, Chengdu 610064, People's Republic of China*
⁴⁰*Soochow University, Suzhou 215006, People's Republic of China*
⁴¹*Southeast University, Nanjing 211100, People's Republic of China*
⁴²*State Key Laboratory of Particle Detection and Electronics, Beijing 100049, Hefei 230026, People's Republic of China*
⁴³*Sun Yat-Sen University, Guangzhou 510275, People's Republic of China*
⁴⁴*Tsinghua University, Beijing 100084, People's Republic of China*
^{45a}*Ankara University, 06100 Tandogan, Ankara, Turkey*
^{45b}*Istanbul Bilgi University, 34060 Eyup, Istanbul, Turkey*
^{45c}*Uludag University, 16059 Bursa, Turkey*
^{45d}*Near East University, Nicosia, North Cyprus, Mersin 10, Turkey*
⁴⁶*University of Chinese Academy of Sciences, Beijing 100049, People's Republic of China*
⁴⁷*University of Hawaii, Honolulu, Hawaii 96822, USA*

⁴⁸University of Jinan, Jinan 250022, People's Republic of China⁴⁹University of Minnesota, Minneapolis, Minnesota 55455, USA⁵⁰University of Muenster, Wilhelm-Klemm-Str. 9, 48149 Muenster, Germany⁵¹University of Science and Technology Liaoning, Anshan 114051, People's Republic of China⁵²University of Science and Technology of China, Hefei 230026, People's Republic of China⁵³University of South China, Hengyang 421001, People's Republic of China⁵⁴University of the Punjab, Lahore-54590, Pakistan^{55a}University of Turin, I-10125, Turin, Italy^{55b}University of Eastern Piedmont, I-15121, Alessandria, Italy^{55c}INFN, I-10125, Turin, Italy⁵⁶Uppsala University, Box 516, SE-75120 Uppsala, Sweden⁵⁷Wuhan University, Wuhan 430072, People's Republic of China⁵⁸Xinyang Normal University, Xinyang 464000, People's Republic of China⁵⁹Zhejiang University, Hangzhou 310027, People's Republic of China⁶⁰Zhengzhou University, Zhengzhou 450001, People's Republic of China

(Received 8 October 2018; published 9 January 2019)

We study the electromagnetic Dalitz decay $J/\psi \rightarrow e^+e^-\eta$ and search for dielectron decays of a dark gauge boson (γ') in $J/\psi \rightarrow \gamma'\eta$ with the two η decay modes $\eta \rightarrow \gamma\gamma$ and $\eta \rightarrow \pi^+\pi^-\pi^0$ using $(1310.6 \pm 7.0) \times 10^6$ J/ψ events collected with the BESIII detector. The branching fraction of $J/\psi \rightarrow e^+e^-\eta$ is measured to be $(1.43 \pm 0.04(\text{stat}) \pm 0.06(\text{syst})) \times 10^{-5}$, with a precision that is improved by a factor of 1.5 over the previous BESIII measurement. The corresponding dielectron invariant mass dependent modulus square of the transition form factor is explored for the first time, and the pole mass is determined to be $\Lambda = 2.84 \pm 0.11(\text{stat}) \pm 0.08(\text{syst}) \text{ GeV}/c^2$. We find no evidence of γ' production and set 90% confidence level upper limits on the product branching fraction $\mathcal{B}(J/\psi \rightarrow \gamma'\eta) \times \mathcal{B}(\gamma' \rightarrow e^+e^-)$ as well as the kinetic mixing strength between the standard model photon and γ' in the mass range of $0.01 \leq m_{\gamma'} \leq 2.4 \text{ GeV}/c^2$.

DOI: 10.1103/PhysRevD.99.012006

I. INTRODUCTION

The study of electromagnetic (EM) Dalitz decays of a vector meson ($V = \rho, \omega, \phi, J/\psi$) into a pseudoscalar meson ($P = \pi^0, \eta, \eta'$) and a lepton-pair, $V \rightarrow \ell^+\ell^-P$ ($\ell = e, \mu$), plays an important role in revealing the structure of hadrons and the interaction mechanism between photons and hadrons [1]. These decays proceed via $V \rightarrow \gamma^*P$ in which the virtual photon γ^* subsequently converts into a lepton pair. Assuming the mesons to be pointlike particles, the dilepton invariant mass ($m_{\ell^+\ell^-}$) dependent decay rate of $V \rightarrow \ell^+\ell^-P$ can be described by quantum electrodynamics (QED) [2]. Any deviation from the QED prediction, caused by the dynamics of the EM structure arising at the $V \rightarrow P$ transition vertex, is formally described by a transition form factor (TFF) [1]. The dependence of the differential decay rate of $V \rightarrow P\ell^+\ell^-$ on the four-momentum transfer squared $q^2 = m_{\ell^+\ell^-}^2$ is parametrized as [1]

$$\begin{aligned} \frac{d\Gamma(V \rightarrow P\ell^+\ell^-)}{dq\Gamma(V \rightarrow P\gamma)} &= \frac{2\alpha}{3\pi q} \left(1 - \frac{4m_\ell^2}{q^2}\right)^{1/2} \left(1 + \frac{2m_\ell^2}{q^2}\right) \\ &\quad \left[\left(1 + \frac{q^2}{m_V^2 - m_P^2}\right)^2 - \frac{4m_V^2 q^2}{(m_V^2 - m_P^2)^2} \right]^{3/2} \\ &\quad \times |F_{VP}(q^2)|^2 \\ &= [\text{QED}(q^2)] \times |F_{VP}(q^2)|^2, \end{aligned} \quad (1)$$

^aAlso at Bogazici University, 34342 Istanbul, Turkey.^bAlso at the Moscow Institute of Physics and Technology, Moscow 141700, Russia.^cAlso at the Functional Electronics Laboratory, Tomsk State University, Tomsk, 634050, Russia.^dAlso at the Novosibirsk State University, Novosibirsk, 630090, Russia.^eAlso at the NRC ‘‘Kurchatov Institute’’, PNPI, 188300, Gatchina, Russia.^fAlso at Istanbul Arel University, 34295 Istanbul, Turkey.^gAlso at Goethe University Frankfurt, 60323 Frankfurt am Main, Germany.^hAlso at Key Laboratory for Particle Physics, Astrophysics and Cosmology, Ministry of Education; Shanghai Key Laboratory for Particle Physics and Cosmology; Institute of Nuclear and Particle Physics, Shanghai 200240, People's Republic of China.ⁱAlso at Government College Women University, Sialkot - 51310, Punjab, Pakistan..^jAlso at Center for Underground Physics, Institute for Basic Science, Daejeon 34126, Korea.

Published by the American Physical Society under the terms of the [Creative Commons Attribution 4.0 International license](#). Further distribution of this work must maintain attribution to the author(s) and the published article's title, journal citation, and DOI. Funded by SCOAP³.

where $\text{QED}(q^2)$ is the QED predicted q^2 dependent decay rate, α is the fine structure constant, $F_{VP}(q^2)$ is the q^2 dependent TFF, and m_ℓ , m_V and m_P are the masses of leptons, V and P mesons, respectively.

The TFFs of light mesons contribute to the hadronic light-by-light (HLBL) corrections [3] to the theoretical determination of the muon anomalous magnetic moment, $a_\mu = (g_\mu - 2)/2$, which provides a low-energy test of the completeness of the standard model (SM) [4,5]. Experimentally, it can directly be accessible by comparing the $m_{\ell^+\ell^-}$ spectrum of Dalitz decays $V \rightarrow \ell^+\ell^-P$ with that of the pointlike QED prediction [1]. Within the vector meson dominance model (VMD) [6], the TFF is mainly governed by the coupling of the γ^* to the V meson via an intermediate vector (V') meson in the timelike region, and is commonly expressed as a multipole function in the charmonium mass region [7]

$$F_{VP}(q^2) = N \sum_{V'} A_{V'} \frac{m_{V'}^2}{m_{V'}^2 - q^2 - i\Gamma_{V'} m_{V'}}, \quad (2)$$

where N is a normalization constant ensuring that $F_{VP}(0) = 1$, V' denotes the intermediate resonances ρ , ω , ϕ , and charmonium vector mesons, $m_{V'}$, $\Gamma_{V'}$ and $A_{V'}$ are the corresponding masses, widths and the coupling constants. The contribution of vector mesons with masses above $(m_V - m_P)$, *nonresonant* contribution, is often represented as

$$F_{VP}(q^2) = \frac{1}{1 - q^2/\Lambda^2}, \quad (3)$$

where Λ is an effective pole mass. The inverse square value Λ^{-2} reflects the slope of the TFF at $q^2 = 0$.

The EM Dalitz decays of light unflavored vector mesons ρ , ω and ϕ are well established by several collider and nuclear physics experiments [8–12]. The BESIII collaboration reported the first measurements of the branching fractions of $J/\psi \rightarrow e^+e^-P$ and the TFF of $J/\psi \rightarrow e^+e^-\eta'$ using a data sample of 225 million J/ψ events [13]. The results agree well with the VMD predictions based on a simple pole approximation [14] within the statistical uncertainties. BESIII has recently accumulated 5 times more statistics of the J/ψ data set [15], which can be used to improve the precision of these measurements and enable measurement of the TFFs of $J/\psi \rightarrow e^+e^-P$.

The EM Dalitz decays can also be utilized to search for a hypothetical dark photon, γ' , via the decay chain $J/\psi \rightarrow \gamma'P$, $\gamma' \rightarrow \ell^+\ell^-$ [14,16]. The γ' is a new type of force carrier in the simplest scenario of an Abelian $U(1)$ interaction under which dark matter particles are considered to be charged [17–19]. A γ' with mass below twice the proton mass can explain the features of the electron/positron excess observed by the cosmic ray experiments [20–23]. A dark photon with such a low mass can also

explain the presently observed deviation of a_μ up to the level of $(3-4)\sigma$ between the measurement and SM prediction [19]. The γ' couples with the SM photon through its kinetic mixing with the SM hypercharge field [24]. The coupling strength between the dark sector and the SM, ϵ , is parametrized as $\epsilon^2 = \alpha'/\alpha$, where α' is the fine structure constant in the dark sector. A series of experiments have reported null results in γ' searches, including the a_μ favored region, and have constrained the ϵ values as a function of γ' mass to be below 10^{-3} [25–27]. More experimental information about the γ' searches via new decay modes, such as $J/\psi \rightarrow \gamma'P$, might be helpful to understand some other possible scenarios of the γ' coupling to the SM [28]. In this paper, we present a study of the EM Dalitz decays $J/\psi \rightarrow e^+e^-\eta$ and search for dielectron decays of a dark photon through $J/\psi \rightarrow \gamma'\eta$ using $(1310.6 \pm 7.0) \times 10^6 J/\psi$ events collected with the BESIII detector [15].

II. THE BESIII EXPERIMENT AND MONTE CARLO SIMULATION

The BESIII detector is a general purpose spectrometer containing four major detector subcomponents with a geometric acceptance of 93% of the total solid angle as described in Ref. [29]. A helium-based (60% He, 40% C_3H_8) multilayer drift chamber (MDC), which contains 43 layers and operates in a 1.0 T (0.9 T) solenoidal magnetic field for the 2009 (2012) J/ψ data, is used to measure the momentum of the charged particles. Charged particle identification (PID) is based on the energy loss (dE/dx) in the tracking system and the time-of-flight (TOF) measured by a scintillation based TOF detector containing one barrel and two endcaps. A CsI(Tl) based electromagnetic calorimeter (EMC) is used to measure the energies of photons and electrons, while a muon counter containing nine (eight) layers of resistive plate chamber counters interleaved with steel in the barrel (endcap) region is used for muon identification.

Monte Carlo (MC) simulated events are used to optimize the event selection criteria, to study the detection acceptance and to understand the potential backgrounds. The GEANT4 [30] based simulation package contains the information about the detector geometry and material description, the detector response and signal digitization models, as well as the records of time dependent detector running conditions and performance. An MC sample of 1.225 billion inclusive J/ψ decays is generated for the background studies with the EVTGEN generator [31] for the known J/ψ decay modes with the branching fractions set to their world average value taken from Ref. [32], and the LUNDCHARM package [33] for the remaining unknown J/ψ decay modes. The KKMC event generator package [34] is used to simulate the production of the J/ψ resonance via e^+e^- annihilation, incorporating the effects of the beam energy spread and initial-state-radiation (ISR).

The angular distribution of the decay $J/\psi \rightarrow e^+e^-\eta$ is simulated according to a combined formula of Eqs. (4) and (6) of Ref. [14], where the dependence on the cosine of the η meson polar angle in the J/ψ rest frame ($\cos\theta_\eta$) is parameterized by $(1 + \alpha_\theta \cos^2\theta_\eta)$ with $\alpha_\theta = 1.0$ measured from the data as described in Sec. III B to take into account of the J/ψ polarization state in the e^+e^- annihilation system, and the TFF is assumed to follow Eq. (3) with $\Lambda = 2.84 \text{ GeV}/c^2$ measured in this analysis also described in Sec. III B. The $J/\psi \rightarrow \gamma'\eta$ decay is modeled by a helicity amplitude model and $\gamma' \rightarrow e^+e^-$ decay by a model of a vector meson decaying to a lepton-pair [31].

III. DATA ANALYSIS

In this analysis, the η meson candidates are reconstructed using the dominant decay modes $\eta \rightarrow \gamma\gamma$ and $\eta \rightarrow \pi^+\pi^-\pi^0$, where the π^0 meson is reconstructed with a $\gamma\gamma$ pair. We select events of interest with two (four) charged tracks with zero net charge in the $\eta \rightarrow \gamma\gamma$ ($\eta \rightarrow \pi^+\pi^-\pi^0$) decay and at least two good photon candidates. The charged tracks are required to be measured in the active region of the MDC, $|\cos\theta| < 0.93$, where θ is the polar angle of the charged tracks. They must also have the points of closest approach to the beam line within ± 10.0 cm from the interaction point in the beam direction and within 1.0 cm in the plane perpendicular to the beam. A PID algorithm, based on energy loss dE/dx in the MDC, TOF information, and energy deposited in the EMC, is performed to identify electrons. An electron-positron pair is required for the selected events. In the decay $J/\psi \rightarrow e^+e^-\eta$, $\eta \rightarrow \pi^+\pi^-\pi^0$, the additional two charged tracks are assumed to be π candidates without any PID requirement.

The photon candidates are reconstructed from the clusters of energy deposits in the EMC that are separated from the extrapolated positions of any charged tracks by more than 10 degrees. The energy of each photon candidate is required to be larger than 25 MeV in the EMC barrel region ($|\cos\theta_\gamma| < 0.8$) or 50 MeV in the EMC endcap regions ($0.86 < |\cos\theta_\gamma| < 0.92$), where θ_γ is the polar angle of the photon. To improve the reconstruction efficiency and energy resolution, the energy deposited in nearby TOF counter is taken into account. The photons reconstructed poorly in the transition region between the barrel and the endcaps are discarded. The EMC timing is required to be within the range of $[0, 700]$ ns to suppress electronic noise and energy deposits unrelated to the event.

The selected charged tracks are constrained to originate from a common vertex point by requiring a successful vertex fit. In order to improve the resolution and further suppress the background, a four-constraint (4C) kinematic fit that imposes overall momentum and energy conservation is implemented for the selected charged tracks and additional two photons under the hypothesis of $J/\psi \rightarrow e^+e^-(\pi^+\pi^-)\gamma\gamma$. The chi-square of the kinematic

fit, χ_{4C}^2 , is required to be less than 100, which rejects about 30% of the background events with a loss of the 10% of the signal events. If there are more than two good photons in an event, we try all the $\gamma\gamma$ combinations, and the one with the least χ_{4C}^2 is chosen. The kinematic variables after the 4C kinematic fit are used in the further analysis. In the decay mode $\eta \rightarrow \pi^+\pi^-\pi^0$, the π^0 candidate is reconstructed with two selected photons by requiring $m_{\gamma\gamma}$ within the range of $[0.08, 0.16] \text{ GeV}/c^2$. The η candidate is reconstructed with the selected $\gamma\gamma$ or $\pi^+\pi^-\pi^0$, respectively, and the corresponding masses ($m_{\gamma\gamma}$ and $m_{\pi^+\pi^-\pi^0}$) are required to be within the range $[0.45, 0.65] \text{ GeV}/c^2$.

With the above selection criteria, the peaking background, which contains an η signal in the final state, is dominated by the events of the radiative decay $J/\psi \rightarrow \gamma\eta$ followed by the conversion of the radiative photon into an e^+e^- pair in the detector material. In order to suppress this background, a photon-conversion finder algorithm [35] is exploited to reconstruct the photon-conversion vertex point. The distance from the conversion vertex point to the origin in the x - y plane, $\delta_{xy} = \sqrt{R_x^2 + R_y^2}$, is used to separate the signal from the gamma conversion events, where R_x and R_y refer to the coordinates of the reconstructed vertex point along the x and y directions, respectively. The scatter plot of R_y versus R_x from the simulated γ conversion background MC sample $J/\psi \rightarrow \gamma\eta$ and the signal MC sample $J/\psi \rightarrow e^+e^-\eta$ is shown in Fig. 1(a), where the circles with radius of 3.5 cm and 6.5 cm correspond to the positions of the beam pipe and inner wall of the MDC, respectively. The corresponding distributions of δ_{xy} from the signal and background MC samples, as well as data events are shown in Fig. 1(b). The δ_{xy} is then required to be less than 2 cm to remove around 98% of the γ conversion events from $J/\psi \rightarrow \gamma\eta$ decay, while retaining about 80% of the signal events $J/\psi \rightarrow e^+e^-\eta$.

In the decay mode $\eta \rightarrow \gamma\gamma$, the background is dominated by the non-peaking background from the QED processes

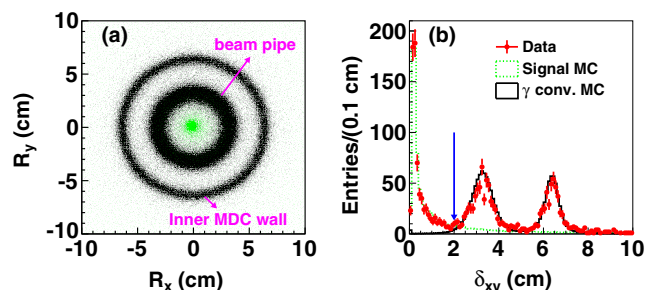


FIG. 1. (a) Scatter plot of R_y versus R_x for the simulated background MC events of $J/\psi \rightarrow \gamma\eta$ (black dot points) and signal MC events of $J/\psi \rightarrow e^+e^-\eta$ (green dot points), and (b) δ_{xy} distribution of signal MC (green dashed line), γ conversion background MC events (black line) and data (red dot error points). The requirement on δ_{xy} is shown by a solid blue arrow.

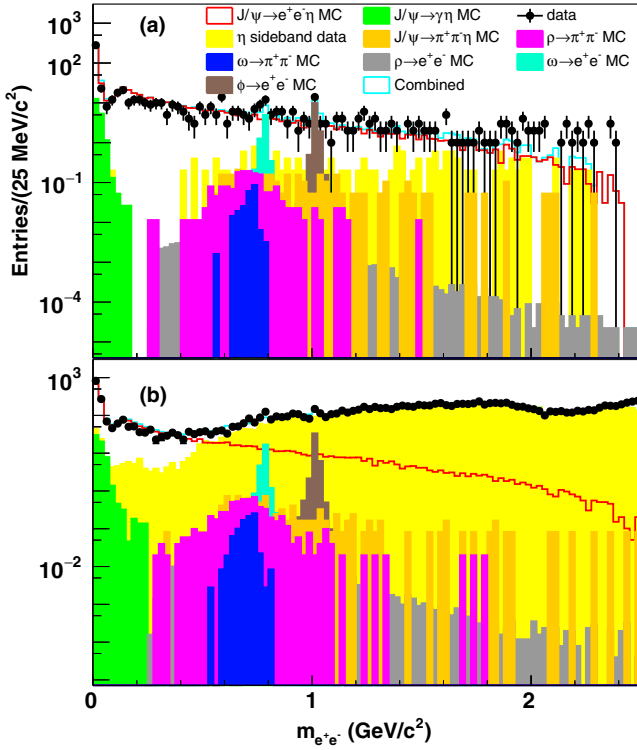


FIG. 2. Spectrum of $m_{e^+e^-}$ from data (black error dot points), signal MC (red), η side-band data (yellow), $J/\psi \rightarrow \gamma\eta$ MC (green), $J/\psi \rightarrow \pi^+\pi^-\eta$ MC (orange), $J/\psi \rightarrow \rho\eta$, $\rho \rightarrow \pi^+\pi^-$ MC (pink), $J/\psi \rightarrow \rho\eta$, $\rho \rightarrow e^+e^-$ MC (brown), $J/\psi \rightarrow \omega\eta$, $\omega \rightarrow \pi^+\pi^-$ MC (blue), $J/\psi \rightarrow \omega\eta$, $\omega \rightarrow e^+e^-$ MC (teal), $J/\psi \rightarrow \phi\eta$, $\phi \rightarrow e^+e^-$ MC (brown), and combined data of MC and side-band (cyan) for the decay modes (a) $\eta \rightarrow \pi^+\pi^-\pi^0$ and (b) $\eta \rightarrow \gamma\gamma$.

$e^+e^- \rightarrow e^+e^-\gamma(\gamma)$ and $e^+e^- \rightarrow 3\gamma$ in which one of the photons converts into an e^+e^- pair. Since the η meson decays isotropically, the cosine of the helicity angle ($\cos\theta_{\text{heli}}$), defined as the angle between the direction of one of the photons and J/ψ direction in the η rest frame, is expected to be uniformly distributed for signal events and to peak near $\cos\theta_{\text{heli}} = \pm 1$ for the background from QED processes. Thus a requirement $|\cos\theta_{\text{heli}}| < 0.9$ is implemented in the decay mode $\eta \rightarrow \gamma\gamma$ to suppress the non-peaking QED background.

After applying the above selection criteria, the distribution of the dielectron invariant mass $m_{e^+e^-}$ of surviving events (within the η signal region $[0.51, 0.58]$ GeV/c^2) is shown in Fig. 2. Besides the EM Dalitz decay of interest, $J/\psi \rightarrow e^+e^-\eta$, small signals of $J/\psi \rightarrow V\eta$ ($V = \rho, \omega, \phi$) with V subsequently decaying into e^+e^- pair are observed. Detailed MC studies indicate that the remaining peaking background is dominated by $J/\psi \rightarrow \gamma\eta$ with γ converting into an e^+e^- pair, which accumulates in the low region of the $m_{e^+e^-}$ distribution. There are also small contributions of the peaking background of $J/\psi \rightarrow \rho/\omega\eta$ with ρ/ω subsequently decaying into a $\pi^+\pi^-$ pair and the direct three body decay $J/\psi \rightarrow \pi^+\pi^-\eta$, in which the $\pi^+\pi^-$ are

misidentified as an e^+e^- pair. The nonpeaking background, which is smoothly distributed in the high mass region of the $m_{e^+e^-}$ distribution, is almost negligible in the decay mode $\eta \rightarrow \pi^+\pi^-\pi^0$, but sizable in the decay mode $\eta \rightarrow \gamma\gamma$ dominated by the radiative Bhabha $e^+e^- \rightarrow \gamma e^+e^-$ process. The distributions of signal and individual background components are also depicted in Fig. 2. Here, the peaking backgrounds are estimated with the MC simulation normalized according to the branching fraction quoted from the PDG [32]; the three body decay $J/\psi \rightarrow \pi^+\pi^-\eta$ is simulated in accordance with the amplitude of $J/\psi \rightarrow \pi^+\pi^-\eta'$ [36]; the non-peaking backgrounds are estimated with the events of data in the η sideband regions, which are defined as $[0.42, 0.50]$ GeV/c^2 and $[0.59, 0.70]$ GeV/c^2 .

A. Branching fraction measurement for the EM Dalitz decays $J/\psi \rightarrow e^+e^-\eta$

In order to suppress the peaking background from $J/\psi \rightarrow V\eta$ with meson V decaying into either the e^+e^- or the $\pi^+\pi^-$ final state, the candidate events within regions of $0.65 < m_{e^+e^-} < 0.90$ GeV/c^2 or $0.96 < m_{e^+e^-} < 1.08$ GeV/c^2 are discarded. The number of remaining peaking background events, estimated by the MC simulation, for both η decay modes after this requirement is summarized in Table I.

In the decay mode $\eta \rightarrow \gamma\gamma$, a sizable nonpeaking background, which is dominated by the radiative Bhabha events $e^+e^- \rightarrow \gamma e^+e^-$ and smoothly distributed in the high region of the $m_{e^+e^-}$ distribution, is suppressed by applying the further requirement $p_{e^\pm} < 1.45$ GeV/c for $m_{e^+e^-} > 0.5$ GeV/c^2 , where p_{e^\pm} is the momentum of the e^\pm charged tracks. Other sources of peaking background are negligible in both η decay modes.

To determine the signal yields, we perform an unbinned extended maximum likelihood (ML) fit to the $m_{\gamma\gamma}$ and $m_{\pi^+\pi^-\pi^0}$ distributions, individually. In the fit, the probability density function (PDF) of the η signal is described with the corresponding signal MC simulated shape convolved with a Gaussian function with parameters that are left free during the fit to take into account the resolution difference between the data and MC simulation. The shape of the nonpeaking

TABLE I. The remaining number of peaking background events in both the η decay modes, where uncertainties are negligible.

Decay process	$\eta \rightarrow \gamma\gamma$	$\eta \rightarrow \pi^+\pi^-\pi^0$
$J/\psi \rightarrow \rho\eta, \rho \rightarrow \pi^+\pi^-$	2.3	0.6
$J/\psi \rightarrow \rho\eta, \rho \rightarrow e^+e^-$	0.4	0.1
$J/\psi \rightarrow \omega\eta, \omega \rightarrow \pi^+\pi^-$	0.1	0.0
$J/\psi \rightarrow \omega\eta, \omega \rightarrow e^+e^-$	0.1	0.0
$J/\psi \rightarrow \phi\eta, \phi \rightarrow e^+e^-$	0.4	0.1
$J/\psi \rightarrow \pi^+\pi^-\eta$	5.2	1.9
$J/\psi \rightarrow \gamma\eta$	61.4	19.5

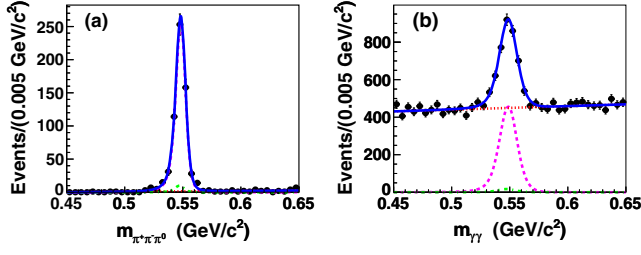


FIG. 3. Results of the unbinned ML fits to the distribution of (a) $m_{\pi^+\pi^-\pi^0}$ and (b) $m_{\gamma\gamma}$, respectively. The non-peaking background contribution is shown by a red dashed curve, the peaking background contribution by a green dashed curve, the signal distribution by a pink dashed curve and the total fit result by a solid blue curve.

background is described by a first order Chebyshev polynomial function with free parameters in the fit. The shape of the peaking background is described by that of MC simulation of the background $J/\psi \rightarrow \gamma\eta$, and the corresponding expected number of events is fixed during the fit. The ML fit yields $N_{\text{sig}} = 594.9 \pm 25.3$ and 1877.2 ± 76.1 events for the decay modes $\eta \rightarrow \pi^+\pi^-\pi^0$ and $\eta \rightarrow \gamma\gamma$, respectively. The corresponding fit curves are shown in Fig. 3. The statistical uncertainty of the extracted signal yield in $\eta \rightarrow \gamma\gamma$ slightly degrades compared to the previous BESIII measurement [13]; this is because the ML fit to the $m_{\gamma\gamma}$ distribution is now performed in the full $m_{e^+e^-}$ range instead of $m_{e^+e^-} < 0.5$ GeV/ c^2 range as required by the previous measurement to avoid the large contamination from the radiative Bhabha background.

B. Transition form factor

Due to large contamination from the radiative Bhabha process in the high $m_{e^+e^-}$ region in the decay mode $\eta \rightarrow \gamma\gamma$, only the events from the $\eta \rightarrow \pi^+\pi^-\pi^0$ decay are used for the TFF study. The vicinities of ω and ϕ in the $m_{e^+e^-}$ distribution are also explored, and the resonant contribution of $J/\psi \rightarrow V\eta$, $V \rightarrow e^+e^-$ is considered as a signal in the TFF measurement. Due to limited statistics in the high mass region as seen in Fig. 2, the TFF is extracted bin-by-bin from the efficiency and branching fractions corrected signal yields for the bin sizes of 0.10 GeV/ c^2 between $2m_e < m_{e^+e^-} < 1.10$ GeV/ c^2 , 0.12 GeV/ c^2 between $1.10 < m_{e^+e^-} < 1.34$ GeV/ c^2 , 0.14 GeV/ c^2 between $1.34 < m_{e^+e^-} < 1.90$ GeV/ c^2 , 0.16 GeV/ c^2 between $1.90 < m_{e^+e^-} < 2.06$ GeV/ c^2 and 0.17 GeV/ c^2 in the remaining $m_{e^+e^-}$ regions with a total 20 bins, where m_e is the mass of the electron. The signal yield in each bin of $m_{e^+e^-}$ is extracted by performing ML fits to the $m_{\pi^+\pi^-\pi^0}$ distribution as described in Sec. III A. The peaking background contribution from the $J/\psi \rightarrow \gamma\eta$ exists only in the first and second bins of $m_{e^+e^-}$. All the peaking background contributions including $J/\psi \rightarrow \gamma\eta$,

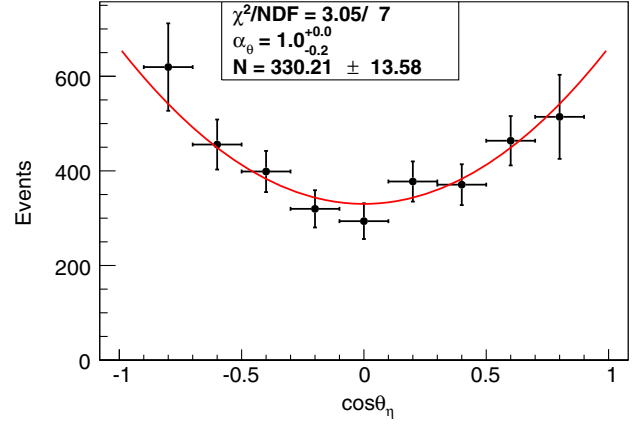


FIG. 4. Fit to the efficiency corrected signal yield versus $\cos\theta_\eta$ for data in the $\eta \rightarrow \pi^+\pi^-\pi^0$ decay mode. The black dots with error bar are data, which include both statistical and systematic uncertainties, and the solid red curve shows the fit results.

$J/\psi \rightarrow \rho/\omega\eta$ ($\rho/\omega \rightarrow \pi^+\pi^-$) and $J/\psi \rightarrow \pi^+\pi^-\eta$ are estimated with the MC simulation and subtracted from the extracted signal yield from the ML fit in each bin.

The signal efficiency for the TFF measurement is calculated by the signal MC sample generated according to the method discussed in Sec. II, but with a constant TFF of $F_{J/\psi\eta}(m_{e^+e^-}) = 1.0$. The angular distribution parameter α_θ , used as an input parameter in this signal MC simulation, is evaluated after extracting the $\cos\theta_\eta$ dependent signal yield with a step size of 0.2 between $-0.9 < \cos\theta_\eta < 0.9$ using a similar procedure of the ML fit mentioned above. Figure 4 shows the efficiency corrected signal yield versus $\cos\theta_\eta$ data and a fit with $\mathcal{N}(1 + \alpha_\theta \cos^2\theta_\eta)$, where \mathcal{N} is a normalization constant and the efficiency for this study is evaluated after generating the simulated signal MC events with a flat distribution in $\cos\theta_\eta$. The angular distribution parameter α_θ is determined to be $1.0^{+0.0}_{-0.2}$ with a condition of $0 \leq |\alpha_\theta| \leq 1.0$ to satisfy the theoretical constraints [37].

Table II summarizes the background subtracted fitted N_{sig}^i and branching fractions $\mathcal{B}(J/\psi \rightarrow e^+e^-\eta)^i$ for all 20 bins. The branching fraction of $J/\psi \rightarrow e^+e^-\eta$ is computed using

$$\mathcal{B}(J/\psi \rightarrow e^+e^-\eta) = \frac{N_{\text{sig}}}{N_{J/\psi} \cdot \mathcal{E} \cdot \mathcal{B}(\eta \rightarrow F)} \quad (4)$$

where \mathcal{E} is the signal selection efficiency, $\mathcal{B}(\eta \rightarrow F)$ is the branching fraction of subsequent η decays taken from the PDG [32] and $N_{J/\psi} = (1310.6 \pm 7.0) \times 10^{-6}$ is the number of J/ψ events from Ref. [15]. The distribution of $\mathcal{B}(J/\psi \rightarrow e^+e^-\eta)^i$ normalized to the $m_{e^+e^-}$ bin size superimposed with the QED predicted branching fractions, computed using the formula of Eq. (1), is shown in Fig. 5.

TABLE II. Fitted N_{sig}^i , differential branching fraction $\mathcal{B}(J/\psi \rightarrow e^+e^-\eta)^i$ and the TFF $|F(q^2)|^2$, described in Sec. V, for all 20 bins. The first uncertainty is statistical and the second systematic discussed in Sec. IV.

$m_{e^+e^-}$ (GeV/ c^2)	N_{sig}^i	$\mathcal{B}(J/\psi \rightarrow e^+e^-\eta)^i$ (10^{-7})	$ F(q^2) ^2$
[$2m_e$, 0.1]	$302.7 \pm 18.1 \pm 19.2$	$84.6 \pm 5.1 \pm 5.4$	$1.12 \pm 0.07 \pm 0.07$
[0.1, 0.2]	$60.9 \pm 7.8 \pm 3.9$	$13.3 \pm 1.7 \pm 0.8$	$1.13 \pm 0.15 \pm 0.07$
[0.2, 0.3]	$40.4 \pm 6.6 \pm 2.6$	$7.4 \pm 1.2 \pm 0.5$	$1.09 \pm 0.18 \pm 0.07$
[0.3, 0.4]	$32.0 \pm 5.7 \pm 2.0$	$5.8 \pm 1.0 \pm 0.4$	$1.21 \pm 0.22 \pm 0.08$
[0.4, 0.5]	$20.6 \pm 4.6 \pm 1.3$	$3.7 \pm 0.8 \pm 0.2$	$1.00 \pm 0.22 \pm 0.06$
[0.5, 0.6]	$31.6 \pm 5.7 \pm 2.0$	$5.6 \pm 1.0 \pm 0.4$	$1.92 \pm 0.34 \pm 0.12$
[0.6, 0.7]	$18.2 \pm 4.5 \pm 1.3$	$3.2 \pm 0.8 \pm 0.2$	$1.33 \pm 0.33 \pm 0.09$
[0.7, 0.8]	$29.8 \pm 5.7 \pm 1.9$	$5.2 \pm 1.0 \pm 0.3$	$2.61 \pm 0.50 \pm 0.17$
[0.8, 0.9]	$19.1 \pm 4.5 \pm 1.2$	$3.2 \pm 0.8 \pm 0.2$	$1.91 \pm 0.45 \pm 0.12$
[0.9, 1.0]	$14.4 \pm 3.9 \pm 0.9$	$2.5 \pm 0.7 \pm 0.2$	$1.72 \pm 0.46 \pm 0.11$
[1.0, 1.1]	$19.8 \pm 4.6 \pm 1.2$	$3.4 \pm 0.8 \pm 0.2$	$2.74 \pm 0.64 \pm 0.17$
[1.1, 1.22]	$14.6 \pm 4.2 \pm 1.0$	$2.5 \pm 0.7 \pm 0.2$	$1.94 \pm 0.56 \pm 0.13$
[1.22, 1.34]	$16.8 \pm 4.1 \pm 1.1$	$2.9 \pm 0.7 \pm 0.2$	$2.75 \pm 0.68 \pm 0.17$
[1.34, 1.48]	$9.7 \pm 3.2 \pm 0.6$	$1.6 \pm 0.5 \pm 0.1$	$1.61 \pm 0.53 \pm 0.10$
[1.48, 1.62]	$12.4 \pm 3.6 \pm 0.8$	$2.1 \pm 0.6 \pm 0.1$	$2.62 \pm 0.77 \pm 0.16$
[1.62, 1.76]	$6.3 \pm 2.7 \pm 0.6$	$1.1 \pm 0.5 \pm 0.1$	$1.74 \pm 0.75 \pm 0.16$
[1.76, 1.90]	$9.1 \pm 3.1 \pm 0.6$	$1.5 \pm 0.5 \pm 0.1$	$3.15 \pm 1.09 \pm 0.20$
[1.90, 2.06]	$10.2 \pm 3.7 \pm 0.6$	$1.9 \pm 0.7 \pm 0.1$	$4.86 \pm 1.74 \pm 0.30$
[2.06, 2.23]	$7.6 \pm 2.8 \pm 0.5$	$1.6 \pm 0.6 \pm 0.1$	$5.96 \pm 2.22 \pm 0.38$
[2.23, 2.40]	$5.7 \pm 2.7 \pm 0.4$	$1.2 \pm 0.6 \pm 0.1$	$8.84 \pm 4.12 \pm 0.65$

C. The dark photon search in $J/\psi \rightarrow \gamma'\eta$ decays

The dark photon search is performed in the full $m_{e^+e^-}$ spectrum using the surviving event candidates within the η mass window [0.51, 0.57] GeV/ c^2 of two η decay modes. A series of unbinned extended ML fits to the $m_{e^+e^-}$ distribution is performed to determine the signal yields as a function of $m_{\gamma'}$ in the interval of $0.01 \leq m_{\gamma'} \leq 2.40$ GeV/ c^2 . In the fit, the signal PDF is the sum of two Crystal Ball (CB) functions, which have common mean and width values, but opposite side tails.

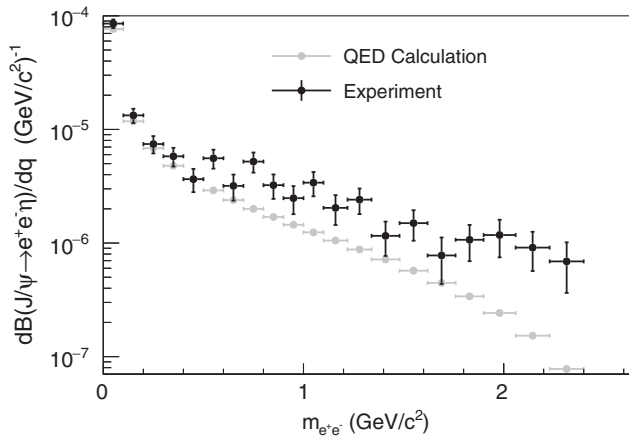


FIG. 5. Differential branching fraction $J/\psi \rightarrow e^+e^-\eta$ as a function of $m_{e^+e^-}$. The black dots with error bars are experimental data, where the error bars include both statistical and systematic uncertainties, and the gray dots with error bars are the MC prediction based on the pointlike QED calculation.

The parameters of the CB are extracted and extrapolated from the simulated signal MC events generated for 27 assumed $m_{\gamma'}$ points while assuming the width of the γ' to be negligible in comparison to the experimental resolution. The background PDF is described by a composite function of polynomial and exponential functions, $f(m_{e^+e^-}) = c_0 \cdot m_{e^+e^-} + c_1 \cdot m_{e^+e^-}^2 + e^{c_2 m_{e^+e^-}}$, for $m_{\gamma'} < 0.2$ GeV/ c^2 , while a second order Chebyshev polynomial function is used in the remaining region. The signal selection efficiency and resolution vary in the range of (5.0–37.0)% ((3.0–18.0)%) and 3–8 MeV/ c^2 , for the decay mode of $\eta \rightarrow \gamma\gamma$ ($\pi^+\pi^-\pi^0$), respectively, depending on the momentum of the e^\pm tracks.

We search for the γ' signal in steps of 2 MeV/ c^2 in the $m_{e^+e^-}$ distribution ranging from 10 MeV/ c^2 to 2.4 GeV/ c^2 excluding the vicinities of the ω and ϕ signals. The parameters of the signal PDF are kept fixed, while the parameters of the background PDF, the number of signal events (N_{sig}) and background events are determined by the fit. In order to address the fit problem associated with low-statistics, a lower bound of N_{sig} is imposed with a requirement that the total signal and background PDF remains non-negative [38]. The statistical signal significance is computed as $\mathcal{S} = \text{sign}(N_{\text{sig}}) \sqrt{-2 \ln(\mathcal{L}_0/\mathcal{L}_{\text{max}})}$, where \mathcal{L}_{max} and \mathcal{L}_0 are the likelihood values when N_{sig} is left free and fixed at 0, respectively, and $\text{sign}(N_{\text{sig}})$ is the sign of N_{sig} . The plots of N_{sig} and signal significance as a function of $m_{\gamma'}$ for both the η decay modes are shown in Fig. 6. The largest local significance is 2.92σ at $m_{\gamma'} = 0.590$ GeV/ c^2 in the $\eta \rightarrow \pi^+\pi^-\pi^0$ decay and 2.98σ at

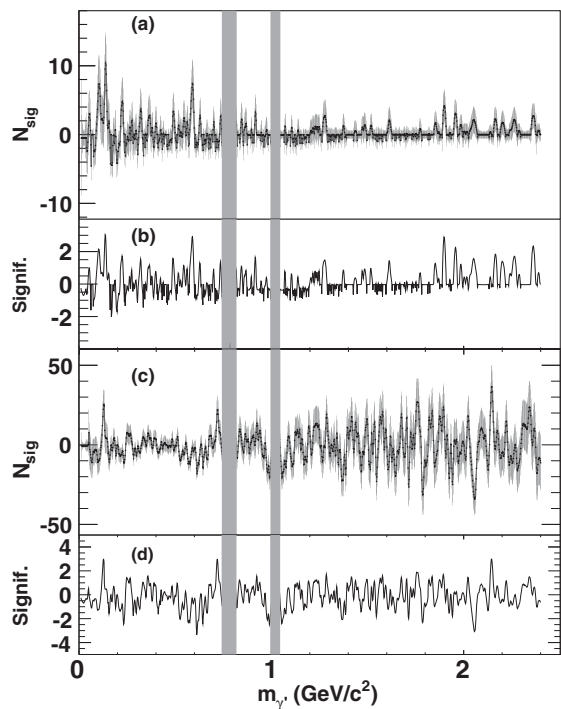


FIG. 6. Number of signal events and statistical signal significance as a function of m_{γ} (a)-(b) for $\eta \rightarrow \pi^+\pi^-\pi^0$ decay and (c)-(d) for $\eta \rightarrow \gamma\gamma$ decay. The shaded regions of ω and ϕ resonances are excluded from the search. The asymmetric behavior in the high m_{γ} region of (a)-(b) is due to constraining the total PDF to be non-negative in the fit.

$m_{\gamma} = 2.144 \text{ GeV}/c^2$ in the $\eta \rightarrow \gamma\gamma$ decay, which are less than 3σ . Therefore, we conclude that no evidence of γ' production is found in both the η decay modes.

IV. SYSTEMATIC UNCERTAINTY

Table III summarizes the sources of additive and multiplicative systematic uncertainties considered in this analysis, where the additive systematic uncertainties arise from the fit procedure including the signal and background modeling, as well as the bias of the fit procedure. The multiplicative systematic uncertainty arises from the systematic uncertainty on the number of J/ψ events, the branching fractions in the cascade decay and the event reconstruction and selection efficiencies.

In the measurements of the branching fraction of $J/\psi \rightarrow e^+e^-\eta$, the signal yields are determined by fitting the corresponding $m_{\gamma\gamma}$ and $m_{\pi^+\pi^-\pi^0}$ distributions, while in the TFF studies, the signal yields are extracted with the same fit procedure in the $m_{\pi^+\pi^-\pi^0}$ distribution only in different $m_{e^+e^-}$ bins. The uncertainty associated with the signal model in the fit is studied by replacing the corresponding PDF to be the sum of two CB functions convolved with a Gaussian function, where the parameters of the CB functions are extracted from fits to the signal MC samples. The uncertainty associated with the peaking background is studied by varying its expected number of events within $\pm 1\sigma$ of the uncertainties in the fit, and

TABLE III. Summary of systematic uncertainties. The systematic uncertainties correlated between the decay modes $\eta \rightarrow \pi^+\pi^-\pi^0$ and $\eta \rightarrow \gamma\gamma$ are denoted by asterisks. Here “Negl.” means negligible, and “...” means the corresponding source of systematic uncertainty is not applicable in a particular decay process.

Source	$J/\psi \rightarrow e^+e^-\eta$			$J/\psi \rightarrow \gamma'\eta$	
	$\eta \rightarrow \gamma\gamma$	$\eta \rightarrow 3\pi$	TFF measurement	$\eta \rightarrow \gamma\gamma$	$\eta \rightarrow 3\pi$
	Additive systematic uncertainties (events)				
Fixed PDFs	8.50	0.9	negligible	0.0–1.0	0.0–0.6
Nonpeaking background	56.0	1.4	0.0–0.6	0.0–12.0	0.0–5.0
Fit Bias	2.0	0.1	0.1	0.1	0.1
Total	56.7	1.7	0.1–0.6	0.1–12.0	0.1–5.0
	Multiplicative systematic uncertainties (%)				
Charged tracks (* for e track only)	2.4	4.4	4.4	2.4	4.4
e^\pm PID*	1.2	1.2	1.2	1.2	1.2
Photon detection efficiency*	2.0	2.0	2.0	2.0	2.0
χ^2_{4C}	0.9	0.9	0.9	0.9	0.9
η/π^0 mass window requirement	...	1.0	1.0	1.0	2.0
Veto of γ conversion*	1.0	1.0	0.0–1.5	0.0–1.5	0.0–1.5
$\cos\theta_\gamma^{\text{hel}}$	1.9	1.9	...
e^\pm momentum	Negl.
TFF	0.2	Negl.	...	0.2	Negl.
$\mathcal{B}(\eta \rightarrow \gamma\gamma)$	0.5	0.5	...
$\mathcal{B}(\eta \rightarrow \pi^+\pi^-\pi^0)$...	1.2	1.2	...	1.2
$\mathcal{B}(J/\psi \rightarrow \gamma\eta)$	3.1	3.1	3.1
$\mathcal{B}(\gamma' \rightarrow e^+e^-)$ *	0.0–14.0	0.0–14.0
Number of J/ψ events*	0.5	0.5	0.5	0.5	0.5
Total	4.1	5.4	6.2–6.3	5.1–15.0	6.4–15.5

observed to be negligible. The uncertainty associated with the nonpeaking background is studied by replacing the corresponding PDF to be a second order Chebyshev polynomial function in the fit. In the fit to search for the γ' boson, the signal is modeled with the sum of two CB function whose parameters are extracted and extrapolated from the simulated MC samples at 27 $m_{\gamma'}$ points. The corresponding uncertainty is studied by changing the parameters of the CB functions within $\pm 1\sigma$ of their uncertainties, taking into account the correlation between the different parameters. The uncertainty due to the background model is studied by changing the order of polynomial functions in the fit. The changes in the signal yields due to the PDF parameters are considered as the uncertainties. To validate the reliability of fits, we produce a large number of pseudoexperiments, which are of the same statistics of data, and perform the same fit procedure in each pseudoexperiment. The resultant average difference between the input and output signal yields is found to be very small and considered as one of the systematic uncertainties.

The tracking efficiency for charged pions is studied with the control sample of $J/\psi \rightarrow \pi^+\pi^-\pi^0$ [39]. The difference between data and MC simulation is found to be 1%, and is considered as the systematic uncertainty of the charged pion. The efficiencies of tracking and PID for e^\pm is explored with the control sample of radiative Bhabha events $e^+e^- \rightarrow \gamma e^+e^-$ in 2-dimensional bins of momentum versus polar angle. The resultant average differences on efficiency between data and MC simulation, 1.2% for tracking and 0.6% for the PID, weighted according to the momentum and polar angle distribution of the MC samples, are considered as the systematic uncertainties.

The photon reconstruction efficiency is studied with a control sample of $e^+e^- \rightarrow \gamma\mu^+\mu^-$, in which the momentum of the ISR photon is inferred from the four-momenta of the $\mu^+\mu^-$ pair [40]. The difference in the efficiency between data and MC simulation is smaller than 1%, which is taken as the systematic uncertainty. In the decay mode $\eta \rightarrow \pi^+\pi^-\pi^0$, the uncertainty related with the π^0 mass window requirement is studied with a high statistics control sample of $J/\psi \rightarrow p\bar{p}\pi^0$ and is assigned to be 1%. In the γ' search, the uncertainty associated with the η mass window requirement is studied with a control sample of $J/\psi \rightarrow p\bar{p}\eta$, and is assigned to be 1%, too.

The uncertainty associated with the 4C kinematic fit is explored by utilizing a control sample of $J/\psi \rightarrow \pi^+\pi^-\pi^0$ in which the π^0 dominant decay modes of $\pi^0 \rightarrow \gamma\gamma$ and $\pi^0 \rightarrow \gamma e^+e^-$ are utilized to mimic the $J/\psi \rightarrow e^+e^-\eta$ signal with subsequent decay modes $\eta \rightarrow \gamma\gamma$ and $\eta \rightarrow \pi^+\pi^-\pi^0$, respectively. The relative difference in efficiencies between data and MC simulation in the corresponding control samples is observed to be up to the level of 0.9%, and considered as the systematic uncertainty.

The control sample of $J/\psi \rightarrow \pi^+\pi^-\pi^0$, $\pi^0 \rightarrow \gamma e^+e^-$ is also utilized to evaluate the systematic uncertainty for the

$\delta_{xy} < 2$ cm requirement used to suppress the γ -conversion background. The simulated MC events for $\pi^0 \rightarrow \gamma e^+e^-$ are generated with a simple monopole approximation TFF, $F(m_{e^+e^-}^2) = 1 + a_\pi m_{e^+e^-}^2/m_{\pi^0}^2$, where m_{π^0} is the nominal π^0 mass and $a_\pi = 0.032 \pm 0.004$ is the slope parameter [32]. We extract the $\pi^0 \rightarrow \gamma e^+e^-$ signal from the data by performing a ML fit to the $m_{e^+e^-}$ distribution before and after the selection of $\delta_{xy} < 2$ cm requirement. The corresponding differences in efficiencies, 1.0% in the measurement of branching fraction of $J/\psi \rightarrow e^+e^-\eta$ and (0.0–1.5)% depending on $m_{e^+e^-}$ in the TFF measurement and γ' search, are taken as the systematic uncertainties.

We similarly utilize the control sample $J/\psi \rightarrow \pi^+\pi^-\pi^0$, $\pi^0 \rightarrow \gamma\gamma$ to evaluate the systematic uncertainty due to the photon helicity angle requirement $|\cos\theta_{\text{heli}}| < 0.9$ in the $\eta \rightarrow \gamma\gamma$ decay. The background in this control sample, $\pi^0 \rightarrow \gamma e^+e^-$, has a flat shape in $m_{\gamma\gamma}$, and is eliminated by performing a ML fit to the $m_{\gamma\gamma}$ distribution. The uncertainty is evaluated to be up to the level of 1.9% by comparing the efficiencies between the data and MC simulation, where the efficiency is the ratio of signal yields with and without this requirement applied. We extract the signal yield in $\eta \rightarrow \gamma\gamma$ decay by varying the requirement of e^\pm momentum within one standard deviation of its statistical uncertainty, and one of the largest values of the relative difference between the signal yields is considered as the systematic uncertainty and found to be negligible.

In the branching fraction measurement of the $J/\psi \rightarrow e^+e^-\eta$ Dalitz decay, the signal MC samples used to evaluate the detection efficiency are generated by following the TFF of Eq. (3) with measured Λ value of 2.84 GeV/ c^2 as described in Sec. III. Two alternative MC samples with values of the pole mass Λ differing by $\pm 1\sigma$ are generated, and the resulting largest relative difference in efficiencies, negligible for the decay mode $\eta \rightarrow \pi^+\pi^-\pi^0$ and 0.2% for the decay mode $\eta \rightarrow \gamma\gamma$, are considered as the systematic uncertainty.

The systematic uncertainties associated with the decay branching fractions of $\eta \rightarrow \pi^+\pi^-\pi^0$ and $\eta \rightarrow \gamma\gamma$ are taken from the PDG [32]. In the measurements of TFF and coupling strength between the dark sector and the SM ϵ , the related uncertainty associated with the branching fraction of $J/\psi \rightarrow \gamma\eta$ is taken from the PDG [32], and in the ϵ measurement, the uncertainty of the theoretical branching fraction $\mathcal{B}(\gamma' \rightarrow e^+e^-)$, dominated by the uncertainty of the R value [32], varies in the range of (0–14)% depending upon the $m_{\gamma'}$ [41]. The uncertainty of the number of J/ψ events is determined to be 0.5% using the inclusive hadronic events of the J/ψ decays [15].

V. RESULTS

We compute the branching fraction of $J/\psi \rightarrow e^+e^-\eta$ in both decay modes of $\eta \rightarrow \gamma\gamma$ and $\eta \rightarrow \pi^+\pi^-\pi^0$ by using Eq. (4). The signal efficiency \mathcal{E} is evaluated to be 26.4% in

decay mode $\eta \rightarrow \gamma\gamma$ and 13.7% in decay mode $\eta \rightarrow \pi^+\pi^-\pi^0$ using the signal MC samples. The branching fraction of $J/\psi \rightarrow e^+e^-\eta$ is determined to be $(1.38 \pm 0.06(\text{stat}) \pm 0.07(\text{syst})) \times 10^{-5}$ in the decay mode $\eta \rightarrow \gamma\gamma$ and $(1.47 \pm 0.06(\text{stat}) \pm 0.08(\text{syst})) \times 10^{-5}$ in the decay mode $\eta \rightarrow \pi^+\pi^-\pi^0$, where the first uncertainties are statistical and second systematic. A weighted average method [42] is used to combine the two branching fraction measurements taking correlated (shown by asterisks in Table III) and uncorrelated systematic uncertainties into account. The combined $\mathcal{B}(J/\psi \rightarrow e^+e^-\eta)$ for both η decay modes is $(1.43 \pm 0.04(\text{stat}) \pm 0.06(\text{syst})) \times 10^{-5}$. Compared with the previous measured value of $1.6 \pm 0.07(\text{stat}) \pm 0.06(\text{syst})$ from BESIII [13], the total (statistical) uncertainty is reduced by a factor of 1.5 (1.8). The central value of the measured branching fraction improves over the previous BESIII measurement [13] due to taking into account of the J/ψ polarization state in the e^+e^- annihilation system during the signal MC simulation.

The TFF in each $m_{e^+e^-}$ bin is determined by dividing $\mathcal{B}(J/\psi \rightarrow e^+e^-\eta)^i$ by the integrated QED prediction in each $m_{e^+e^-}$ interval (Table II). Figure 7 shows a plot of the resultant TFF versus $m_{e^+e^-}$. A chi-square fit to the TFF versus $m_{e^+e^-}$ data is performed using a modified multipole function of Eq. (2), in which the contributions of the ρ resonance and nonresonance are included, and the interference is neglected:

$$|F_{J/\psi\eta}(q^2)|^2 = |A_\rho|^2 \left(\frac{m_\rho^2}{(m_\rho^2 - q^2)^2 + \Gamma_\rho^2 m_\rho^2} \right)^2 + |A_\Lambda|^2 \left(\frac{1}{1 - q^2/\Lambda^2} \right)^2, \quad (5)$$

where the mass and width of the ρ resonance are fixed to the values in the PDG [32]. The statistical uncertainties and

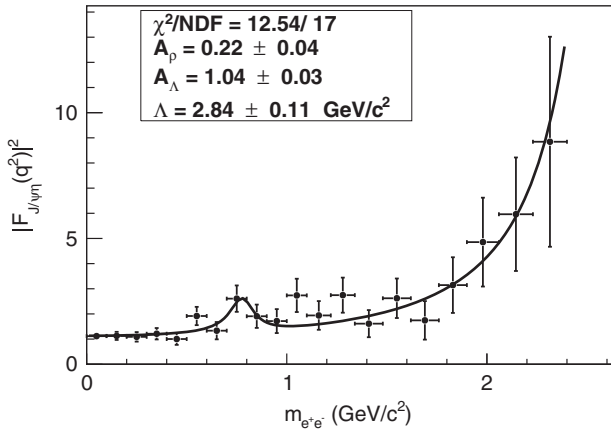


FIG. 7. Fit to the TFF versus $m_{e^+e^-}$ for data. The black dots with error bar are data, which include both statistical and systematic uncertainties, and the solid black curve shows the fit results.

uncorrelated systematic uncertainty (between the different $m_{e^+e^-}$ bins) are considered when building the chi-square function. The fit curve is depicted in Fig. 7, too. The statistical significance of the ρ signal is 4.0σ estimated with the change of chi-square values with and without ρ signal included in the fit. We fit the TFF of data once again by including the interference between ρ and nonresonant components. The resultant change on Λ , $0.05 \text{ GeV}/c^2$, is taken to be one of the systematic uncertainties. We also fit the TFF of data without including the systematic uncertainty, the resultant change on Λ , $0.06 \text{ GeV}/c^2$, is taken as another systematic uncertainty. Finally, the pole mass is determined to be $\Lambda = 2.84 \pm 0.11(\text{stat}) \pm 0.08(\text{syst}) \text{ GeV}/c^2$.

We compute the upper limits on the product branching fraction $\mathcal{B}(J/\psi \rightarrow \gamma'\eta) \times \mathcal{B}(\gamma' \rightarrow e^+e^-)$ at the 90% confidence level (C.L.) as a function of $m_{\gamma'}$ using a Bayesian method after incorporating the systematic uncertainty by smearing the likelihood curve with a Gaussian function with a width of the systematic uncertainty. The combined result is obtained by adding the logarithm likelihoods of two η decays by taking into account their correlated and uncorrelated systematic uncertainties. As shown in Fig. 8(a), the combined limits on product branching fraction $\mathcal{B}(J/\psi \rightarrow \gamma'\eta) \times \mathcal{B}(\gamma' \rightarrow e^+e^-)$ vary in the range of $(1.9 - 91.1) \times 10^{-8}$

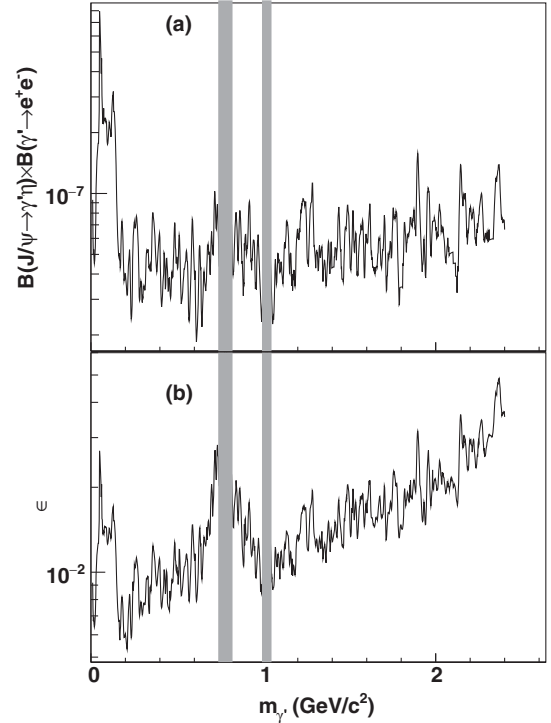


FIG. 8. The combined upper limits at the 90% C.L. on (a) product branching fraction $\mathcal{B}(J/\psi \rightarrow \gamma'\eta) \times \mathcal{B}(\gamma' \rightarrow e^+e^-)$ and (b) coupling strength (ϵ) between the SM and dark sector as a function of $m_{\gamma'}$ for both η decay modes. The regions of ω and ϕ resonances shaded by gray lines are excluded from the γ' search.

for $0.01 \leq m_{\gamma'} \leq 2.4 \text{ GeV}/c^2$ depending on $m_{\gamma'}$ points. The upper limit on $\mathcal{B}(J/\psi \rightarrow \gamma'\eta)$ at the 90% C.L. at each $m_{\gamma'}$ point is computed by dividing the combined upper limit on the product branching fraction $\mathcal{B}(J/\psi \rightarrow \gamma'\eta) \times \mathcal{B}(\gamma' \rightarrow e^+e^-)$ by the expected dark photon decay branching fraction of $\gamma' \rightarrow e^+e^-$ obtained from Ref. [41]. We then compute the upper limits of the coupling strength between the dark sector and the SM ϵ at the 90% C.L. as a function of $m_{\gamma'}$ using the Eq. (4.6) of Ref. [16], where the TFF is given by Eq. (3) with $\Lambda = 2.84 \text{ GeV}/c^2$. As shown in Fig. 8(b), the upper limits on ϵ at the 90% C.L. vary in the range of 10^{-2} – 10^{-3} for $0.01 \leq m_{\gamma'} \leq 2.4 \text{ GeV}/c^2$ depending on $m_{\gamma'}$.

VI. SUMMARY

In summary, with a data sample of (1310.6 ± 7.0) million J/ψ events collected with the BESIII detector, we study the EM Dalitz decay of $J/\psi \rightarrow e^+e^-\eta$ and search for a dark photon in $J/\psi \rightarrow \gamma'\eta$ decay using two different η decay modes $\eta \rightarrow \gamma\gamma$ and $\eta \rightarrow \pi^+\pi^-\pi^0$. The branching fraction of $J/\psi \rightarrow e^+e^-\eta$ is measured to be $(1.43 \pm 0.04(\text{stat}) \pm 0.06(\text{syst})) \times 10^{-5}$, which supersedes the previous BESIII measurement [13]. We present the first measurement of TFF as a function of $m_{e^+e^-}$ for the decay $J/\psi \rightarrow e^+e^-\eta$. The corresponding pole mass of the TFF is determined to be $\Lambda = 2.84 \pm 0.11(\text{stat}) \pm 0.08(\text{syst}) \text{ GeV}/c^2$ by fitting the TFF versus $m_{e^+e^-}$ data with a modified TFF function. No evidence of dark photon γ' production is observed, and we set upper limits on the product branching fraction $\mathcal{B}(J/\psi \rightarrow \gamma'\eta) \times \mathcal{B}(\gamma' \rightarrow e^+e^-)$ at the 90% C.L. to be in the range of $(1.9\text{--}91.1) \times 10^{-8}$ for $0.01 \leq m_{\gamma'} \leq 2.4 \text{ GeV}/c^2$ depending on $m_{\gamma'}$. The upper limits on the coupling strength between the dark sector and the SM ϵ at the 90% C.L. are also set at the level of 10^{-2} – 10^{-3} , which are above the existing stringent experimental results [25–27].

ACKNOWLEDGMENTS

The BESIII collaboration thanks the staff of BEPCII, the IHEP computing center and the supercomputing center of USTC for their strong support. This work is supported in part by National Key Basic Research Program of China under Contract No. 2015CB856700; National Natural Science Foundation of China (NSFC) under Contracts Nos. 11235011, 11322544, 11335008, 11375170, 11275189, 11425524, 11475164, 11475169, 11625523, 11605196, 11605198, 11635010, 11705192; the Chinese Academy of Sciences (CAS) Large-Scale Scientific Facility Program; the CAS Center for Excellence in Particle Physics (CCEPP); Joint Large-Scale Scientific Facility Funds of the NSFC and CAS under Contracts Nos. U1332201, U1532257, U1532258, U1532102; CAS under Contracts Nos. KJCX2-YW-N29, KJCX2-YW-N45, QYZDJ-SSW-SLH003; 100 Talents Program of CAS; National 1000 Talents Program of China; INPAC and Shanghai Key Laboratory for Particle Physics and Cosmology; German Research Foundation DFG under Contracts Nos. Collaborative Research Center CRC 1044, FOR 2359; Istituto Nazionale di Fisica Nucleare, Italy; Joint Large-Scale Scientific Facility Funds of the NSFC and CAS; Koninklijke Nederlandse Akademie van Wetenschappen (KNAW) under Contract No. 530-4CDP03; Ministry of Development of Turkey under Contract No. DPT2006K-120470; National Natural Science Foundation of China (NSFC); National Science and Technology fund; The Swedish Research Council; U.S. Department of Energy under Contracts Nos. DE-FG02-05ER41374, DE-SC-0010118, DE-SC-0010504, DE-SC-0012069; University of Groningen (RuG) and the Helmholtzzentrum fuer Schwerionenforschung GmbH (GSI), Darmstadt; WCU Program of National Research Foundation of Korea under Contract No. R32-2008-000-10155-0.

-
- [1] L. G. Landsberg, *Phys. Rep.* **128**, 301 (1985).
 - [2] N. M. Kroll and W. Wada, *Phys. Rev.* **98**, 1355 (1955).
 - [3] G. Colangelo, M. Hoferichter, B. Kubis, M. Procura, and P. Stoffer, *Phys. Lett. B* **738**, 6 (2014); G. Colangelo, M. Hoferichter, M. Procura, and P. Stoffer, *J. High Energy Phys.* **09** (2015) 074.
 - [4] F. Jegerlehner and A. Nyffeler, *Phys. Rep.* **477**, 1 (2009).
 - [5] A. Nyffeler, *Phys. Rev. D* **94**, 053006 (2016).
 - [6] J. J. Sakurai, *Currents and Mesons* (University of Chicago, Chicago, 1969).
 - [7] V. M. Budnev and V. A. Karnakov, *Pis'ma Zh. Eksp. Teor. Fiz.* **29**, 439 (1979) [*JETP Lett.* **29**, 398 (1979)].
 - [8] R. R. Akhmetshin *et al.* (CMD-2 Collaboration), *Phys. Lett. B* **613**, 29 (2005).
 - [9] R. Arnaldi *et al.* (NA60 Collaboration), *Phys. Lett. B* **677**, 260 (2009).
 - [10] M. N. Achasov *et al.* (SND Collaboration), *Phys. Lett. B* **504**, 275 (2001).
 - [11] D. Babusci *et al.* (KLOE-2 Collaboration), *Phys. Lett. B* **742**, 1 (2015); A. Anastasi *et al.* (KLOE-2 Collaboration), *Phys. Lett. B* **757**, 362 (2016).
 - [12] P. Adlarson *et al.* (A2 Collaboration), *Phys. Rev. C* **95**, 035208 (2017).
 - [13] M. Ablikim *et al.* (BESIII Collaboration), *Phys. Rev. D* **89**, 092008 (2014).

- [14] J. Fu, H. B. Li, X. Qin, and M. Z. Yang, *Mod. Phys. Lett. A* **27**, 1250223 (2012).
- [15] M. Ablikim *et al.* (BESIII Collaboration), *Chin. Phys. C* **41**, 013001 (2017).
- [16] M. Reece and L. T. Wang, *J. High Energy Phys.* **07** (2009) 051.
- [17] N. Arkani-Hamed, D. P. Finkbeiner, T. R. Slatyer, and N. Weiner, *Phys. Rev. D* **79**, 015014 (2009).
- [18] D. P. Finkbeiner and N. Weiner, *Phys. Rev. D* **76**, 083519 (2007).
- [19] M. Pospelov, *Phys. Rev. D* **80**, 095002 (2009).
- [20] P. Jean *et al.*, *Astron. Astrophys.* **407**, L55 (2003).
- [21] O. Adriani *et al.* (PAMELA Collaboration), *Nature (London)* **458**, 607 (2009).
- [22] M. Ackermann *et al.* (Fermi LAT Collaboration), *Phys. Rev. Lett.* **108**, 011103 (2012).
- [23] M. Aguilar *et al.* (AMS Collaboration), *Phys. Rev. Lett.* **110**, 141102 (2013).
- [24] B. Holdom, *Phys. Lett. B* **166**, 196 (1986).
- [25] J. P. Lees *et al.* (BABAR Collaboration), *Phys. Rev. Lett.* **113**, 201801 (2014).
- [26] J. R. Batley *et al.* (NA48/2 Collaboration), *Phys. Lett. B* **746**, 178 (2015).
- [27] M. Ablikim *et al.* (BESIII Collaboration), *Phys. Lett. B* **774**, 252 (2017).
- [28] P. Fayet, *Eur. Phys. J. C* **77**, 53 (2017).
- [29] M. Ablikim *et al.* (BESIII Collaboration), *Nucl. Instrum. Methods Phys. Res., Sect. A* **614**, 345 (2010).
- [30] S. Agostinelli *et al.* (GEANT4 Collaboration), *Nucl. Instrum. Methods Phys. Res., Sect. A* **506**, 250 (2003).
- [31] D. J. Lange, *Nucl. Instrum. Methods Phys. Res., Sect. A* **462**, 152 (2001); R. G. Ping, *Chin. Phys. C* **32**, 599 (2008).
- [32] M. Tanabashi *et al.* (Particle Data Group), *Phys. Rev. D* **98**, 030001 (2018).
- [33] J. C. Chen, G. S. Huang, X. R. Qi, D. H. Zhang, and Y. S. Zhu, *Phys. Rev. D* **62**, 034003 (2000).
- [34] S. Jadach, B. F. L. Ward, and Z. Was, *Phys. Rev. D* **63**, 113009 (2001).
- [35] Z. R. Xu and K. L. He, *Chin. Phys. C* **36**, 742 (2012).
- [36] M. Ablikim *et al.* (BESIII Collaboration), *Phys. Rev. D* **96**, 112012 (2017).
- [37] M. Claudson, S. L. Glashow, and M. B. Wise, *Phys. Rev. D* **25**, 1345 (1982); C. Carimalo, *Int. J. Mod. Phys. A* **02**, 249 (1987).
- [38] J. P. Lees *et al.* (BABAR Collaboration), *Phys. Rev. D* **87**, 031102(R) (2013).
- [39] M. Ablikim *et al.* (BESIII Collaboration), *Phys. Rev. D* **83**, 112005 (2011).
- [40] V. Prasad, C. X. Liu, X. B. Ji, W. D. Li, H. M. Liu, and X. C. Lou, *Springer Proc. Phys.* **174**, 577 (2016).
- [41] B. Batell, M. Pospelov, and A. Ritz, *Phys. Rev. D* **79**, 115008 (2009).
- [42] G. Cowan, *Statistical Data Analysis* (Oxford University Press, New York, 1998); G. D'Agostini, *Nucl. Instrum. Methods Phys. Res., Sect. A* **346**, 306 (1994).